Journal of
Nanoscience and Nanotechnology
Vol. 13, 781–786, 2013

Fabrication and Properties of Dual-Level Hierarchical Structures Mimicking Gecko Foot Hairs

Peng Zhang[1], Shiyuan Liu[1, 2, *], and Hao Lv[2]

[1] *State Key Laboratory of Digital Manufacturing Equipment and Technology, Huazhong University of Science and Technology, Wuhan 430074, China*
[2] *Wuhan National Laboratory for Optoelectronics, Huazhong University of Science and Technology, Wuhan 430074, China*

RESEARCH ARTICLE

In nature, geckos have extraordinary adhesive capabilities. The multi-scale hierarchical structure of the gecko foot hairs, especially the high-aspect-ratio structure of its micro-scale seta and nano-scale spatulae is the critical factor of the gecko's ability to adopt and stick to any different surface with powerful adhesion force. In this paper, we present a simple and effective approach to fabricate dual-level hierarchical structures mimicking gecko foot hairs. Polydimethyl-siloxane (PDMS) hierarchical arrays were fabricated by demolding from a double stack mold that was composed of an SU-8 mold by thick film photolithography and a silicon mold by inductively coupled plasma (ICP) etching. Top pillars of the fabricated structures have 3 μm diameter and 18 μm in height, while base pillars have 25 μm diameter and 40 μm in height. The water droplet contact angle tests indicate that the hierarchical structures increase the hydrophobic property significantly compared with the single-level arrays and the unstructured polymers, exhibiting superhydrophobicity (154.2°) like the Tokay gecko's (160.9°). The shear force tests show that the top pillars make attachment through side contact with a value of about 0.25 N/cm^2, and moreover, the hierarchical structures are demonstrated to be more suitable for contacting with rough surfaces.

Keywords: Gecko Foot Hairs, Hierarchical Structures, Double Stack Mold, Adhesion, Superhydrophobicity, Shear Force.

1. INTRODUCTION

It is highly desirable to develop a kind of dry adhesive fully based on van der Waals' force due to its wide applications in the deployment and disassembly of micro-electromechanical system (MEMS) devices such as wall-climbing robots, micro-manipulation, and micro-assembly. The extraordinary adhesive characteristics of the geckos in nature show an excellent example and inspire human for design and fabrication of a new kind of biomimetic dry adhesive. The multi-scale hierarchical structure of the gecko foot-hairs, especially the high-aspect-ratio structure of its micro-scale seta and nano-scale spatulae is the critical factor of the gecko's ability to adopt and stick to any different surface with powerful adhesion force.[1, 2]

In recent years, hierarchical structures of different dimensions have been fabricated by several different methods.[3] For example, Campo and Greiner fabricated well-defined arrays of hierarchical microfibrils by multistep photolithography using SU-8 photoresist, and the fabricated top pillars had 9 μm diameter and 35 μm in height.[4] Greiner et al. obtained hierarchical polydimethyl-siloxane (PDMS) arrays by softmolding PDMS onto SU-8 templates, which were fabricated by double-exposure photolithography.[5] The obtained top pillars had a radius of 5 μm and an aspect ratio of 1, and its adhesive property was shown to be even worse than the single-level ones. Murphy et al. made the top fibers by soft lithography and base fibers by capillary molding, and then obtained the hierarchical structure through a curing step.[6] The tests of normal force show that the dual-level structures did increase the adhesive property.

In this paper, we propose a simple and effective method for fabricating high-aspect-ratio dual-level microfiber arrays. The dual-level PDMS microfiber arrays were fabricated by demolding from a double stack mold, which was composed of an SU-8 mold by thick film photolithography and a silicon mold by inductively coupled plasma (ICP) etching. The hydrophobic and adhesive properties of the dual-level microfiber arrays were tested and made comparisons with those of the single-level ones and the unstructured polymers.

*Author to whom correspondence should be addressed.

2. EXPERIMENTAL DETAILS

2.1. Fabrication Process of Dual-Level Microfiber Arrays

Figure 1 shows the schematic processes of the fabrication procedure for dual-level microfiber arrays. First, a silicon master template was fabricated by ICP etching process. The silicon master was covered with equilateral triangular microhole arrays with 3–5 μm diameter and 20–30 μm in depth, which determined the diameters and heights of the top-level pillars. Then, an SU-8 photoresist layer was spun on the silicon master at 500 r/min for 15 s followed by 2000 r/min for 120 s. The estimated thickness of this layer was about 40 μm, which determined the heights of the base-level pillars. After being prebaked for 40 min, the unexposed SU-8 layer was exposed under ultravoilet (UV) light for about 45 s. The mask used for this photolithography process was also covered with equilateral triangular dot arrays with a diameter of 25 μm. Then the whole template was postbaked for about 30 min to reduce the mechanical stress produced by the photolithography process. The next developing process took about 10 min and the double stack mold was formed. To make the demolding process easier, the double stack mold was evaporated with hexamethyl-disilazane (HMDS) as a release agent, which increased the silicon master surface activity and reduced the surface tension. Liquid PDMS prepolymers and curing agent were poured over the mold and cured at 100 °C for 30 min. Finally, the dual-level microfiber arrays were fabricated through a demolding process.

In addition, several single-level microfiber arrays were also fabricated through an ICP process, and they were used to make comparison with the dual-level ones.

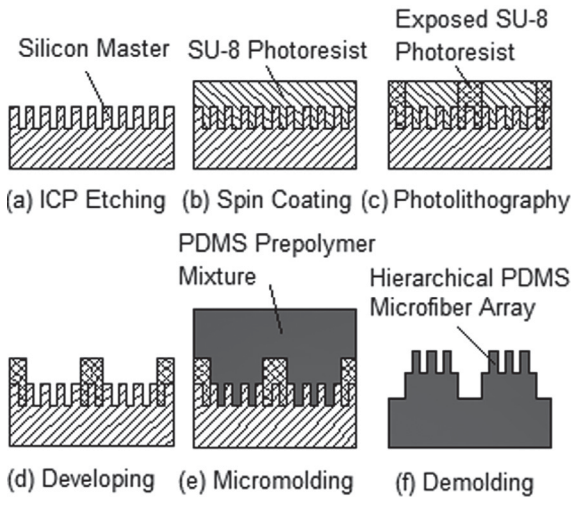

Fig. 1. Schematic processes of fabrication procedure for dual-level microfiber arrays.

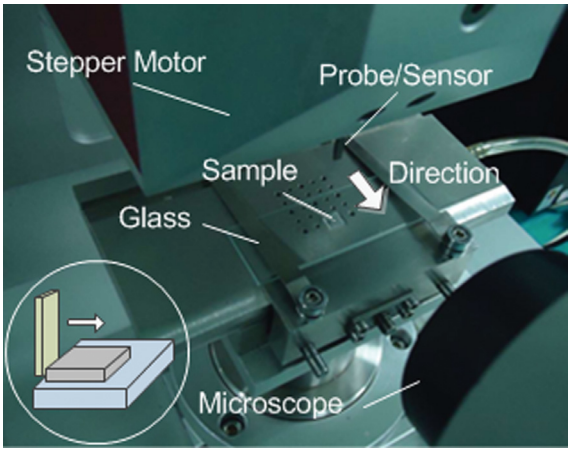

Fig. 2. Testing platform for adhesion property. The shear force of the sample on a glass slide is measured by a probe while the sample is pushed.

2.2. Properties Tests of Dual-Level Microfiber Arrays

The hydrophobic property tests of the dual-level microfiber arrays were performed by a contact angle meter. Water droplet contact angles on unstructured and single-level samples were also measured for comparison.

The adhesive properties of different samples were tested by an XYZ Condor measurement, as shown in Figure 2. The testing platform is composed of a microscope, a stepper motor and a probe. All samples were cut into 10×10 mm^2 pieces and placed on a glass slide held in position by clamps. There were two glass slides in total: one was polished with root mean square roughness $Rq < 0.1$ μm, and the other was depolished with $Rq > 10$ μm. A normal preload of 0.05 N was applied on the samples by counterweight to wipe out any wrinkle of the backing, and would be removed before testing. Then the tip of the probe was located beside the sample with the help of microscope. During testing, the probe was driven to push the sample at a contrast speed of 100 μm/s. Meanwhile, the shear force and the probe displacement were obtained with the help of sensor in probe. The measurement has an accuracy of 0.1%.

3. RESULTS AND DISCUSSION

3.1. Structures of Fabricated Dual-Level Microfiber Arrays

Dual-level microfiber arrays were fabricated with different aspect ratios. The scanning electron microscopy (SEM) image of a low-aspect-ratio structure was shown in Figure 3(a). As we can see, the base pillars have 25 μm diameter and 40 μm in height, while the top pillars have 5 μm diameter and 15 μm in height. Figure 3(b) exhibits the pattern of the arrays. It shows clearly that each base

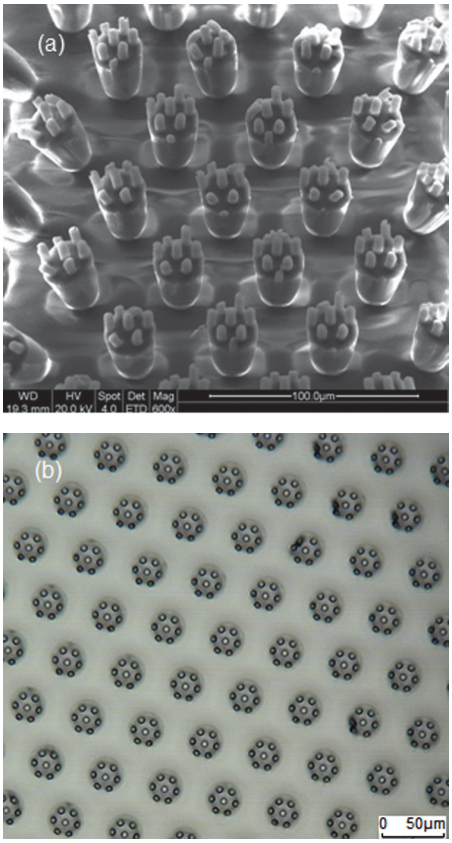

Fig. 3. (a) SEM image and (b) metallurgical microscopy image of the lower aspect-ratio dual-level arrays. The top pillars have 5 μm diameter and 15 μm in height, and the base pillars have 25 μm diameter and 40 μm in height.

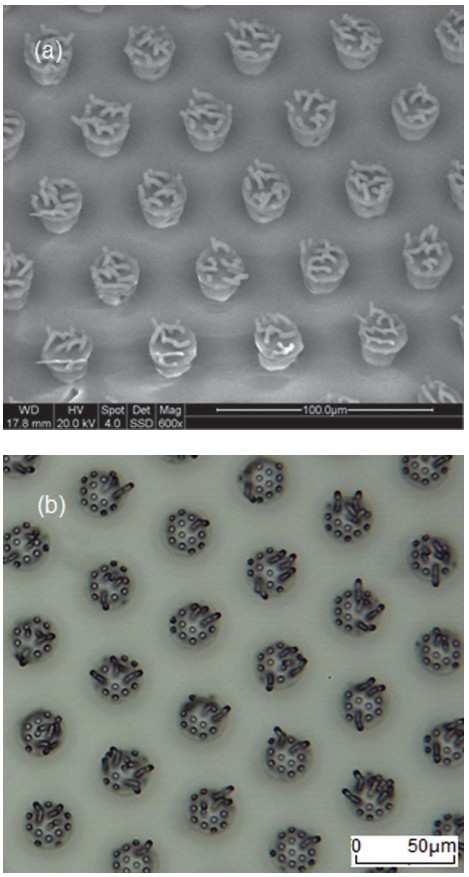

Fig. 4. (a) SEM image and (b) metallurgical microscopy image of the higher aspect-ratio dual-level arrays. The top pillars have 3 μm diameter and 18 μm in height, and the base pillars have 25 μm diameter and 40 μm in height.

pillar has 7 top pillars on it, and all the pillars are in equilateral triangle arrangement without bunch. As the aspect ratio of top pillars gets higher, tips of adjacent pillars begin to bunch as shown in Figure 4(a), where the top pillars have 3 μm diameter and 18 μm in height. It can be seen from Figure 4(b) that each base pillar has about 16 top pillars, and some top pillars have bunched together, while some else incline in different directions due to the uneven stress distribution during demolding. More pillars will bunch together when the aspect ratio is more than 7.

The critical pillar length of microfiber array with anti-bunching condition can be estimated by[7, 8]

$$L_{\max} = \left[\frac{\pi^4 ER}{2^{11}\gamma(1-\nu^2)}\right]^{1/12}\left(\frac{12ER^3w^2}{\gamma}\right)^{1/4} \quad (1)$$

where R is the radius of pillars; w is the pillar space; E, v and γ are the Young's modulus, Poisson ratio and surface energy of pillars, respectively. Therefore, for the top pillars shown in Figure 4 with $R = 1.5$ μm, $w = 3$ μm, $E = 1.8$ Mpa, $v = 0.45$, and $\gamma = 21.6$ mJ/m^2,[9, 10] the critical length $L_{\max}$ is expected theoretically to be 15.6 μm. Actually, the top pillars have a length of 18 μm, which has exceeded the the critical value, resulting in the bunching of the pillars. It also indicates that PDMS is not suitable to fabricate very high aspect-ratio microfiber arrays because of its low Young's modulus.

It is interesting to note that the hierarchical structures we obtained have smaller size and higher aspect-ratio in comparison with those reported by Campo and Greiner et al.[4, 5] This is due to the fact that they made the top pillars directly through masked irradiation on an SU-8 layer, or through demolding from an SU-8 mold made by photolithography process, but we fabricated the top pillars with PDMS through demolding from a silicon template formed by ICP process. Silicon is more suitable to fabricate high aspect-ratio micro/nano-scale structures than SU-8.

The SEM image of a single-level microfiber array sample is shown in Figure 5. The pillars are in equilateral triangle arrangement with diameters of 5∼8 μm and aspect ratios of 5∼6.

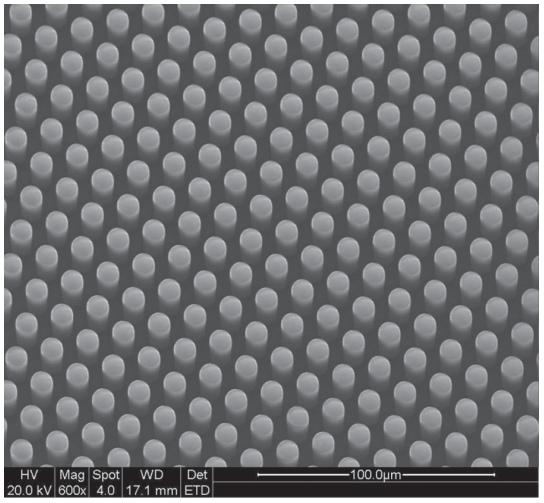

Fig. 5. SEM image of a single-level array. The pillars have 8 μm diameter and 40 μm in height.

3.2. Hydrophobic Properties of Dual-Level Microfiber Arrays

Geckos are able to keep their feet clean while walking about. This self-clean ability can be explained by the lotus effect. The surface of gecko pad appears to be superhydrophobic, with a water droplet contact angle of 160.9°.[11] Thus, the dirt particles on gecko foot hairs can be picked up easily by water droplets, leaving the surface clean.[12]

Observed water droplet contact angles of different samples are shown in Figure 6. As we can see, the single-level arrays increase the water droplet contact angle significantly from 102.7° to 131.7°, while the dual-level arrays achieve a higher contact angle of 154.2°. The dual-level structures exhibit superhydrophobicity like gecko foot hairs. Detailed data of the tests is shown in Table I. It is interesting to note that samples with similar patterns have similar contact angle, and sizes of fibers seem to have little influence on contact angle.

We try to explain the hydrophobic properties of samples by Cassie-Baxter equation. If a water droplet does not entirely wet the rough surface and leaves pockets of air between the droplet and the substrate, the water droplet contact angle of the surface is given by[13, 14]

$$\cos\theta_{\mathrm{CB}} = f\cos\theta_W + (1-f)\cos\theta_{\mathrm{air}} \tag{2}$$

where f is the fraction of the droplet actually in contact with the surface, θ_W is the contact angle on a smooth surface, and θ_{air} is the contact angle with air. Water droplet has a 180° contact angle with air, so this expression can be simplied as

$$\cos\theta_{\mathrm{CB}} = f(1+\cos\theta_W) - 1 \tag{3}$$

Obviously, the contact angle is influenced by the fraction of the contact area, which is determined by the pattern

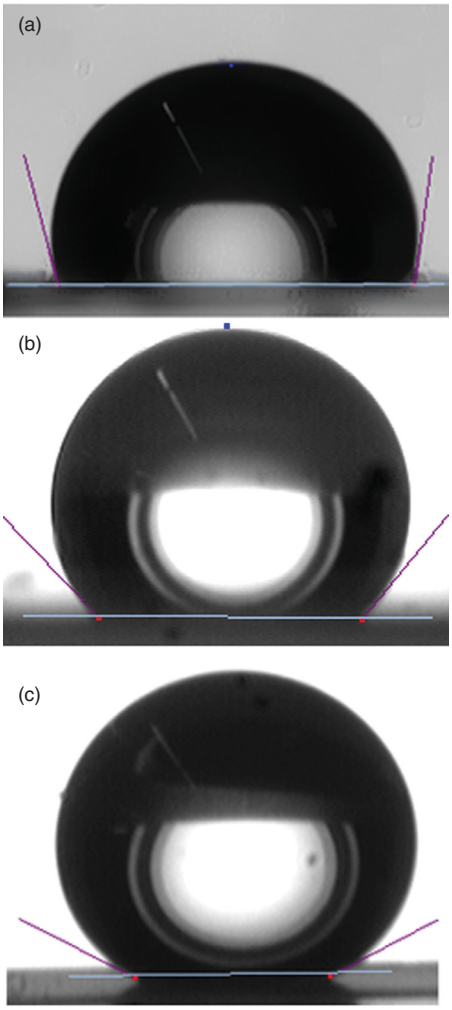

Fig. 6. Observed water droplet contact angle on (a) unstructured PDMS surface (102.7°), (b) single-level PDMS array (131.7°), and (c) dual-level PDMS arrays (154.2°).

of surface. Figure 7 shows the patterns of the single-level and dual-level arrays (with top pillars having 3 μm in diameter), from which the contacting area fraction f can be calculated as $2\pi/9\sqrt{3}$ for single-level arrays and $6\sqrt{3}\pi/625$ for dual-level arrays (with each base pillar

Table I. Observed water contact angle on different structures.

Structures	Diameter (μm) (top level/ base level)	Length (μm) (top level/ base level)	Contact angle (°)
Unstructured surface			102.7
Single-level array	5	30	136.9
	6	30	134.3
	8	40	131.7
Dual-level arrays	3/25	18/40	154.2
	5/25	15/40	151.5
Tokay gecko			160.9

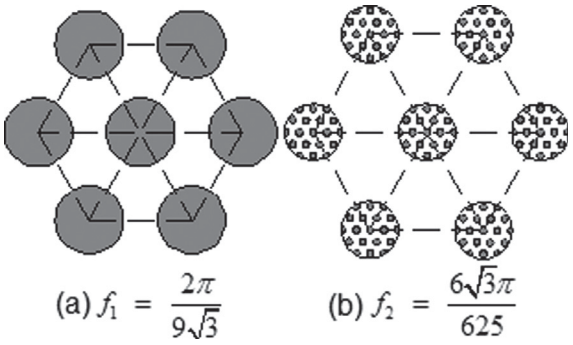

Fig. 7. Contact area fraction of (a) single-level array and (b) dual-level arrays.

having about 16 top pillars as shown in Figure 4). Taking $\theta_W = 102.7°$, we can calculate the contact angle $\theta_{CB} = 133.3°$ for single-level arrays and $\theta_{CB} = 163.6°$ for dual-level arrays. The calculated contact angle of single-level arrays is extremely similar to observed ones, while the value of dual-level arrays has a little error due to the incline of pillars which increases the contact area.

3.3. Adhesion Properties of Dual-Level Microfiber Arrays

Figure 8(a) shows the shear force of the 3 μm dual-level microfiber arrays (with top pillars having 3 μm in diameter) on a polished glass ($Rq < 0.1$ μm) under a preload of 0.05 N. Initially, the shear force increased as the sample was pushed. After reaching a maximum value, the shear force decreased and tended towards stability with a value of 0.25 N. It can be estimated that the sample did not slide until the shear force exceeded the maximum value, and the appearance of this peak is due to the fact that the sample was moved by pushing rather than pulling. The tensile adhesion force is a strong function of normal preload for many microfiber arrays.[15, 16] Thus we measured the shear force of the 3 μm dual-level arrays with different preloads. The results are shown in Figure 8(b), which indicate that the preload did not significantly affect the shear force. A possible reason is that the sizes or Young's modulus of their fibers are much larger than ours, which result in the adhesion way being tip contact rather than side contact. Similar observations were also proved by the experiments of Lee et al.[17, 18]

Figure 9 shows the shear forces of different structures on a polished glass ($Rq < 0.1$ μm) and a depolished glass ($Rq > 10$ μm) respectively. It is noted from Figure 9(a) that the dual-level arrays have poor performance on the smooth surface, compared with the single-level arrays and the unstructured polymers. However, as the roughness of the contacting surface increases, the adhesion forces for the unstructured polymers decreases significantly, and that for the single-level arrays decreases obviously as well. As a comparison, the adhesion force for the dual-level arrays is influenced slightly, as shown in Figure 9(b). This is because that when contacting with a smooth surface, the dual-level arrays can only make the contact by top-pillars, and the contact area is less than those of the

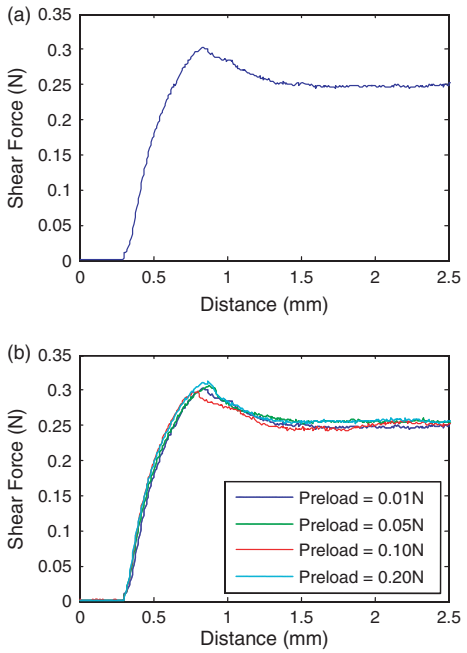

Fig. 8. (a) Shear force of the 3 μm dual-level microfiber arrays on a polished glass, and (b) shear forces under different preloads.

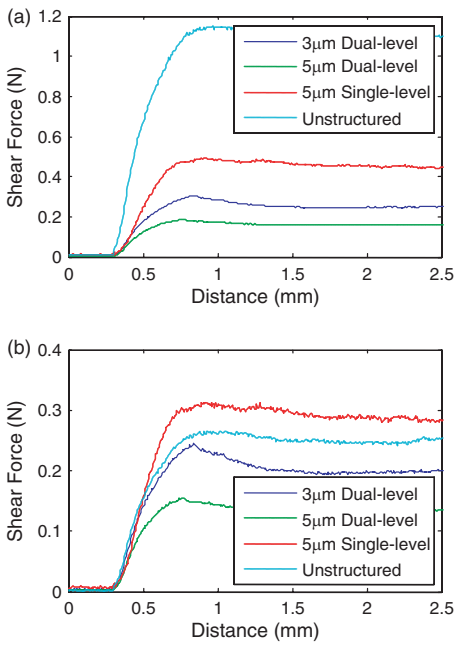

Fig. 9. Shear forces of different structures on (a) a polished glass and (b) a depolished glass under the same preload of 0.05 N.

RESEARCH ARTICLE

unstructured polymers and the sing-level arrays. However, when contacting with a rough surface under the same preload, the dual-level arrays can make contact much easier than single-level ones and the unstructured polymers, as the hierarchical property decreases the stiffness of the whole structures. This observation was proved by Kim and Bhushan's multi-scale spring model,[19, 20] which has demonstrated that hierarchical structures are more suitable for contacting with rough surfaces. Even so, here we have to point out that due to the small fraction of arrays, the dual-level structures in Figure 9(b) still have a worse performance than other structures.

4. CONCLUSION

In summary, we have presented a simple method for fabricating high aspect-ratio dual-level microfiber arrays by combining photolithography, ICP etching, and micromolding processes. The top pillars of the fabricated hierarchical arrays have 3 μm diameter and 18 μm in height, while the base pillars have 25 μm diameter and 40 μm in height. In addition, we take an anti-bunching equation to explain the bunching of pillars. The water droplet contact angle tests indicate that the hierarchical arrays increase the hydrophobic property significantly compared with single-level arrays and unstructured polymers. The hierarchical arrays exhibit superhydrophobicity (154.2°) like the Tokay gecko's (160.9°), which is explained by Cassie-Baxter equation. The shear force tests show that the top pillars make attachment through side contact with a value of about 0.25 N/cm^2, and moreover, the hierarchical structures are demonstrated to be more suitable for contacting with rough surfaces. This is due to the fact that the hierarchical property structures decreases the stiffness of the whole structures and the roughness has a smaller effect on the hierarchical structures.

Acknowledgments: This work was supported by the National Natural Science Foundation of China (Grant Nos. 91023032, 51005091, and 50775090) and the National Instrument Development Specific Project of China (Grant No. 2011YQ160002).

References and Notes

1. K. Autumn, Y. Liang, T. Hsieh, W. Zesch, W. P. Chan, T. Kenny, R. Fearing, and R. J. Full, *Nature* 405, 681 **(2000)**.
2. K. Autumn, A. Dittmore, D. Santos, M. Spenko, and M. Cutkosky, *J. Exp. Biol.* 209, 3569 **(2006)**.
3. L. F. Boesel, C. Greiner, E. Arzt, and A. Del Campo, *Adv. Mater.* 22, 2125 **(2010).**
4. A. del Campo and C. Greiner, *J. Micromech. Microeng*. 17, R81 **(2007)**.
5. C. Greiner, E. Arzt, and A. del Campo, *Adv. Mater*. 21, 479 **(2009).**
6. M. Murphy, S. Kim, and M. Sitti, *ACS Appl. Mater. Interfaces* 1, 849 **(2009)**.
7. H. Gao, X. Wang, H. Yao, S. Gorb, and E. Arzt, *Mech. Mater*. 37, 275 **(2005)**.
8. S. Y. Liu, P. Zhang, X. Cheng, R. Malik, and Z. R. Tang, *Adv. Sci. Lett*. 4, 1546 **(2011)**.
9. K. M. Choi and J. A. Rogers, *J. Am. Chem. Soc.* 125, 4060 (2003).
10. D. K. Armani and C. Liu, *J. Micromech. Microeng*. 10, 80 **(2000)**.
11. W. R. Hansen and K. Autumn, *Proc. Natl. Acad. Sci. USA* 102, 385 **(2005)**.
12. S. Sethi, L. Ge, L. Ci, P. M. Ajayan, and A. Dhinojwala, *Nano Lett*. 8, 322 **(2008)**.
13. A. B. D. Cassie and S. Baxter, *Trans. Faraday Soc*. 40, 546 **(1944)**.
14. R. N. Wenzel, *Phys. Chem.* 53, 1466 **(1949)**.
15. S. Kim and M. Sitti, *Appl. Phys. Lett*. 89, 261911 **(2006)**.
16. S. Gorb, M. Varenberg, and A. Peressadko, *J. R. Soc. Interface* 4, 271**(2007)**.
17. J. Lee, C. Majidi, B. Schubert, and R. S. Fearing, *J. R. Soc. Interface* 5, 835 **(2008)**.
18. B. Schubert, J. Lee, C. Majidi, and R. S. Fearing, *J. R. Soc. Interface* 5, 845 **(2008)**.
19. T. W. Kim and B. Bhushan, *J. Adhes. Sci. Technol*. 21, 1 **(2007)**.
20. B. Bhushan, *J. Adhes. Sci. Technol*. 21, 1213 **(2007)**.

Received: 12 September 2011. Accepted: 30 November 2011.